

1 This is a Preprint and has not been peer reviewed.

2

3 **Title**

4 Relative role of rock erodibility and sediment load in setting channel slope of mountain  
5 rivers

6

7 **Author**

8 Naoya O. Takahashi

9 Department of Earth science, Graduate school of Science, Tohoku University

10 [naoya.takahashi.c5@tohoku.ac.jp](mailto:naoya.takahashi.c5@tohoku.ac.jp)

11

12 **Abstract**

13

14 Rock strength influences channel slope by altering substrate erodibility and  
15 the size of sediments supplied to the channels. Although the frequent  
16 presence of knickpoints at lithological boundaries indicates that rock  
17 erodibility significantly determines channel morphology, a growing body of  
18 field evidence suggests that the coarse sediment supply from hard rock units  
19 is a primary factor in channel steepening. To assess the relative effects of  
20 rock erodibility and imposed sediment load on channel slope, five rivers in  
21 Tsugaru, northern Japan were studied, where these rivers flow through  
22 alternating harder volcanic rock and softer sedimentary rock. The minimum  
23 channel slope required to transport both *in situ* sediments and those  
24 supplied from upstream was calculated. The findings suggest that sediment  
25 effects largely account for the observed variations in channel slope across  
26 both volcanic and sedimentary rocks. The proportion of channel slope  
27 irrelevant to the imposed sediment load was slightly higher in volcanic rock  
28 reaches than in sedimentary rock reaches, which can be attributed to the  
29 lower erodibility of volcanic rock. Considering the grain size distributions of  
30 volcanic and sedimentary rock particles and the calculated impacts of  
31 sediment load, it is argued that the coarse sediment supply from volcanic  
32 rock is the primary cause of the difference in channel steepness between the  
33 rock types in Tsugaru. Although this conclusion holds generally true across

34 Tsugaru, certain reaches with locally high channel steepness exhibit more  
35 extensive bedrock exposure than adjacent gentler reaches, suggesting that  
36 contrasts in erodibility also play a significant role in determining the channel  
37 slope. Therefore, examining what factors alter the relative significance of  
38 rock erodibility and sediment load can enhance our understanding of how  
39 rock properties influence longitudinal stream profiles.

40

41 **Keywords:** *Rock strength, erodibility, sediment load, grain size*

42

## 43 **1 INTRODUCTION**

44 Bedrock properties significantly control topography and the rate of landscape change.  
45 In erosional landscapes, the morphology of channels and erosion rates are associated  
46 with rock erodibility, which depends on rock properties such as the degree of fracturing  
47 and tensile strength (Molnar et al., 2007; Sklar & Dietrich, 2001; DiBiase et al., 2018a;  
48 Turowski et al., 2023). Longitudinal stream profiles are typically steeper in rocks with  
49 low erodibility, allowing erosion to occur at rates comparable to those in rocks with  
50 higher erodibility or to align with the rate of baselevel changes (Hack, 1973; Howard &  
51 Kirby, 1983; Duvall et al., 2004; Bursztyn et al., 2015; Harel et al., 2016; Yanites et  
52 al., 2017). Although rock erodibility is crucial in the evolution of fluvial landscapes, it  
53 does not always manifest in stream profiles. This discrepancy is partly because other  
54 factors such as climate, tectonics, and sediment dynamics might offset the effects of  
55 differential erodibility or exert a more dominant influence on channel slopes (Whipple &  
56 Tucker, 2002; Kirby et al., 2003; Sklar & Dietrich, 2006; Takahashi et al., 2022;  
57 Leonard et al., 2023). Moreover, landscape evolution models have demonstrated that  
58 the apparent disconnect between rock erodibility and channel slope or erosion rates can  
59 result only from the contrast in erodibility when rivers carve through layered rocks with  
60 varying erodibilities (Forte et al., 2016; Perne et al., 2017). Thus, understanding how  
61 and to what extent rock strength determines channel slope is essential for identifying  
62 the drivers of landscape evolution.

63 Rock strength indirectly influences the channel slopes by affecting the size of sediment  
64 produced on hillslopes. The rivers flowing through bedrock typically become steeper as  
65 they transport a larger volume of sediment downstream because of the need to expose  
66 and incise the bedrock (Hack, 1957; Sklar & Dietrich, 2006; Shobe et al., 2021; Carr et  
67 al., 2023; Sklar, 2024). To assess the impact of sediment load on channel slope, Sklar

68 and Dietrich (2006) calculated the minimum channel slope required to entrain bed  
69 materials and transport sediment from upstream to downstream. They explored how  
70 the proportion of the channel slope attributable to the imposed sediment load varied  
71 with the rock tensile strength based on the saltation–abrasion river incision model.  
72 Unlike river incision models that exclude the effects of sediment (e.g., detachment-  
73 limited model), their model predicted that channel slope remained relatively unchanged  
74 with variations in rock tensile strength, with sediment load playing a dominant role in  
75 influencing channel slope. Subsequent studies incorporating sediment terms into river  
76 incision models have confirmed a less pronounced impact of rock strength on channel  
77 slope compared to predictions from models that disregard the sediment effects  
78 (Turowski et al., 2007; Guryan et al., 2024). Hard rocks tend to produce larger, denser,  
79 and more durable grains than soft rocks (e.g., Attal & Lavé, 2009; Sklar et al., 2017),  
80 leading to a longer residence time in channels and a potentially greater impact on  
81 channel slope—a finding that is supported by numerous studies (e.g., Duvall et al.,  
82 2004; Johnson et al., 2009; Thaler & Covington, 2016; Finnegan et al., 2017; Shobe et  
83 al., 2021a; Lai et al., 2021; Anderson et al., 2023). Thaler and Covington (2016)  
84 observed that the normalized channel steepness increased with both boulder size and  
85 the areal fraction of boulder coverage in rivers cutting through bedrock of varying  
86 mechanical strengths. Lai et al. (2021) reported that the channels in softer sedimentary  
87 rocks became steeper when receiving coarse sediments from upstream volcanic rock  
88 units. These observations suggest that the influence of coarse sediment from upstream  
89 hard rock units persists even after transitioning to softer bedrock, affecting the  
90 disparity in channel slopes between rock types.

91 This study assessed the relative impacts of rock erodibility and imposed sediment load  
92 on channel morphology to reveal how rock type influences river morphodynamics.

93 Following the methodologies of Sklar and Dietrich (2006) and Lai et al. (2021), I  
94 calculated the minimum channel slope required to transport the imposed sediment load,  
95 using hydraulic geometry and grain size data from five rivers draining areas with harder  
96 volcanic rock and softer sedimentary rock units in Northern Japan. The findings  
97 indicated that sediment effects could account for most of the variation in channel slope  
98 across both rock types. Additionally, the proportion of the slope component not related  
99 to sediment load was found to be larger in reaches of volcanic rock compared to those  
100 of sedimentary rock, which was attributed to differences in rock erodibility. The  
101 discussion then explores how rock erodibility and sediment load govern the slopes of  
102 mountain rivers.

103

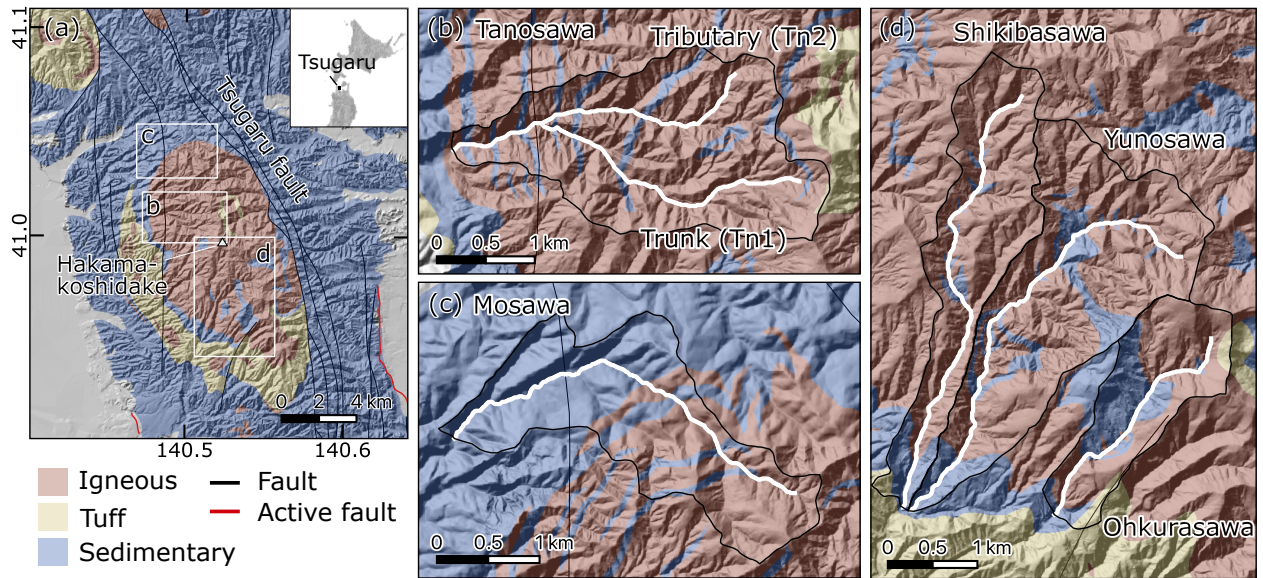
## 104 **2 Geologic setting**

105 Tsugaru Mountain is located in northern Japan and primarily comprises Neogene  
106 sedimentary and volcanic rocks, including shale, mudstone, and sandstone (Figure 1).  
107 Around Hakamakoshi-dake, which has the peaks with an elevation of approximately  
108 630 m, basalt and dolerite have intruded into the Miocene sedimentary rocks, creating  
109 a dome structure near the headwaters (Tsushima & Uemura, 1959; Uemura et al.,  
110 1959; Fujii, 1981; Nemoto, 2014). The basaltic rocks display various forms; some are  
111 massive and joint-free, whereas others are densely jointed or deeply weathered (Figure  
112 2). The Tsugaru Fault is a west-dipping reverse fault trending north-south that is  
113 situated on the eastern flank of Hakamakoshi-dake, separating the basaltic dome to the  
114 west from the Plio-Pleistocene sedimentary rocks to the east (Uemura et al., 1959;  
115 Nemoto, 2014). Active since the late Pliocene, this fault has continued its activity up to  
116 the deposition of the Tsurugasaka formation at 0.76 Ma (Suzuki et al., 2005; Mimura,  
117 1979; Nemoto, 2014). With a vertical displacement exceeding 1000 m, the fault has

118 caused the adjacent sedimentary and volcanic layers to tilt westward (Mimura, 1979;  
119 Ujiie et al., 2006). Currently, the deformation front is located at the eastern base of the  
120 mountain range (Headquarters for Earthquake Research Promotion, 2004).

121 This study examines five rivers on the western flank of Tsugaru Mountain (Figure 1).  
122 The river courses, specifically Mosawa, Shikibasawa, Yunosawa, and Ohkurasawa,  
123 alternate between volcanic and sedimentary rocks. The channel slopes of these rivers  
124 are generally steeper over volcanic substrates than sedimentary ones (Figure 3;  
125 Supporting Information Figure S1). However, certain sections such as in Yunosawa  
126 exhibit a decoupling between channel slope and substrate type, indicating that  
127 substrate erodibility may not solely determine longitudinal stream profiles.

128 In Tanosawa, another surveyed river, the presence of sedimentary rock is minimal.  
129 Both the main stream and a tributary of Tanosawa traverse similar basaltic formations,  
130 yet the main stream, Tn1, exhibits a steeper gradient than the tributary, Tn2 (Figure  
131 3a), suggesting that the channel slope variations are influenced by factors other than  
132 rock erodibility. Understanding why Tn1 is steeper than Tn2 could reveal the factors  
133 influencing channel slope dependency on rock type. Therefore, Tanosawa was included  
134 in this study. It was hypothesized that the observed slope differences might be caused  
135 by the variations in bed material size, resulting from spatial heterogeneity in rock  
136 fracturing (Figure 2). To test this hypothesis and quantify the impact of the sediment  
137 on the channel slope, the same survey methodology was applied in Tanosawa as in the  
138 other four rivers.



139

140 Figure 1. Geology of the study area. Faults and active faults are after Geological survey  
 141 of Japan (2023) and Nakata & Imaizumi (2002), respectively. (a) Geologic map is  
 142 modified after a 1:200,000 map (Geological survey of Japan, 2023). Inset: location of  
 143 the Tsugaru Mountain. (b–d) River sections and their catchment areas investigated in  
 144 this study. Geologic map is modified after 1:50,000 maps (Tsushima & Uemura, 1959;  
 145 Uemura et al., 1959; Fujii, 1981).

146



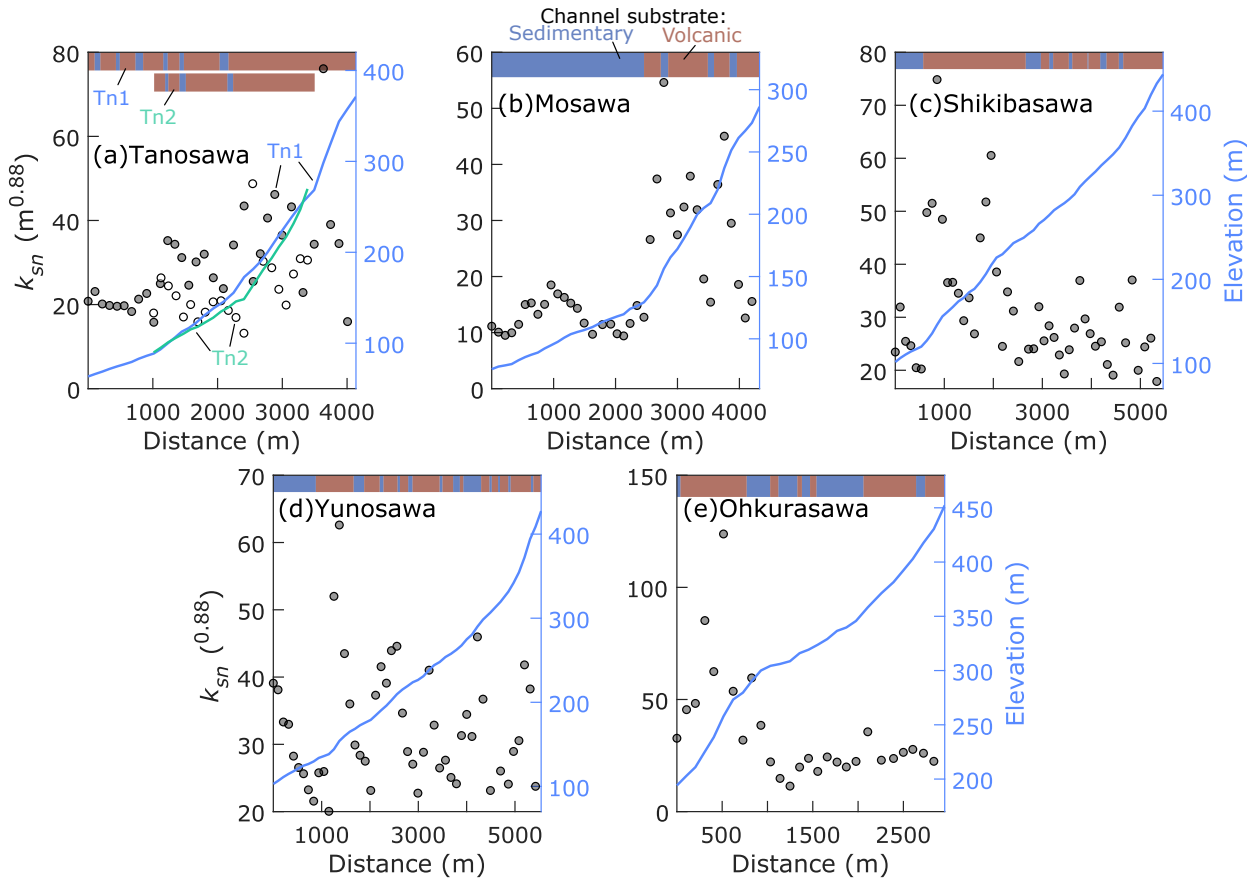


147

148 Figure 2. Bedrock outcrops of basalt. (a) Densely jointed bedrock exposed in a stream

149 channel. Length of hammer: ~30 cm. (b) Bedrock outcrop with minor surficial cracks.

150



151  
 152 Figure 3. Normalized channel steepness (circles) and longitudinal profiles (lines) along  
 153 the studied sections. Bar at the top represents channel substrate. (a) Gray and white  
 154 circles represent normalized channel steepness of the trunk stream (Tn1) and the  
 155 tributary (Tn2). Blue and green lines are stream profiles of Tn1 and Tn2.

156  
 157 **3 Method**

158 To investigate the influence of rock strength on channel slope, I calculated normalized  
 159 channel steepness ( $k_{sn}$ ), hillslope angles along the stream, and normalized wideness of  
 160 channels ( $k_{wn}$ ). Additionally, a slope component analysis was conducted, which  
 161 segmented the current channel slope into two components associated with the imposed  
 162 sediment load and a third component unrelated to the sediment load (Sklar and  
 163 Dietrich, 2006). It was hypothesized that the proportion of slope components

164 associated with the sediment load would decrease as the erosional resistance of the  
165 rock increased. This hypothesis was tested by comparing the proportions of slope  
166 components associated with the sediment load between reaches composed of volcanic  
167 and sedimentary rocks.

168

### 169 **3.1 Topographic analysis**

170 We calculated the normalized channel steepness,  $k_{sn}$ , using a 10-m-meshed digital  
171 elevation model (DEM) provided by the Geospatial Information Authority in Japan and  
172 the Topotoolbox (Schwanghart and Scherler, 2014),

$$173 \quad k_{sn} = SA^{\theta_{ref}}, \quad (1)$$

174 where  $A$  denotes the upstream catchment area, and  $\theta_{ref}$  indicates a reference  
175 concavity index (Snyder et al., 2000). The river reaches were segmented every 100 m  
176 along the streams, and the average channel slope and catchment area were computed  
177 for each of these 100-m-long segments. A reference concavity of 0.44 was employed,  
178 as determined by linear regression of all stream data in the log S-log A space  
179 (Supporting Information Figure S1). The analysis focused on river sections with a  
180 drainage area greater than 0.4 km<sup>2</sup>, excluding colluvial reaches (Supporting  
181 Information Figure S1f; Stock and Dietrich, 2003). A one-sided Wilcoxon rank-sum test  
182 was conducted for each river to determine if  $k_{sn}$  values differed significantly between  
183 sedimentary and volcanic rock reaches at a 5% significance level. The null hypothesis  
184 posited that sedimentary rock reaches exhibited smaller  $k_{sn}$  values than volcanic rock  
185 reaches.

186 The variations in hillslope angles along the trunk streams were analyzed to assess their  
187 impact on channel steepness, as these angles influence the rates and processes of  
188 hillslope sediment supply (Roering et al., 2001; Montgomery & Brandon, 2002). The

189 hillslopes connected directly to the trunk stream were initially mapped based on slope  
190 aspect derived from the 10-m-meshed DEM. These hillslopes were then subdivided  
191 every 200 m along the streams, and the 16th, 50th, and 84th percentile values of  
192 hillslope angles were calculated.

193 High-flow width  $W$  was measured using a TruPulse®200 laser range finder (Laser  
194 Technology, Inc) and the normalized wideness  $k_{wn}$  was calculated for each site (Allen  
195 et al., 2013).

$$196 \quad k_{wn} = WA^{-b_{ref}} \quad (2)$$

197 Width measurements were conducted to determine the maximum and minimum values  
198 at the site, and  $k_{wn}$  was calculated using the mean value. As it is not possible to  
199 measure the width during a flood, flood debris, washed out tree roots, vegetation limits,  
200 and channel bank heights were used as references (Whittaker et al., 2007). The  
201 exponent  $b_{ref}$  was estimated by fitting the following equation to data obtained from  
202 each river:

$$203 \quad W = k_w A^b \quad (3)$$

204 where  $k_w$  denotes a coefficient and  $b$  represents an exponent that is used as  $b_{ref}$ .

205

### 206 **3.2 Slope component analysis**

207 To assess the impact of sediment load on longitudinal channel profiles, I conducted a  
208 slope component analysis following the methodologies of Sklar & Dietrich (2006) and  
209 Lai et al. (2021). For bedrock incision to occur, the channel slope must be sufficiently  
210 steep to transport both the sediments from the riverbed and those transported from  
211 upstream reaches and expose bedrock. Based on this premise, Sklar and Dietrich  
212 (2006) decomposed the steady-state channel slope into three components:

$$213 \quad S = S_{D_s} + \Delta S_{Q_s} + \Delta S_E, \quad (4)$$

214 where  $S_{D_s}$  denotes the threshold slopes for the incipient motion of the bed materials.  
 215  $\Delta S_{Q_s}$  indicates the additional slope above  $S_{D_s}$  to transport sediment supplied from  
 216 upstream.  $\Delta S_E$  indicates the residual slope.  $S_{D_s}$  denotes the slope that makes the  
 217 Shields number for a sediment particle ( $\tau^*$ ) equal to the critical Shields number ( $\tau_c^*$ ).

$$218 \quad \tau^* = \frac{SR}{R_b D_s} \quad (5)$$

$$219 \quad S_{D_s} = \frac{\tau_c^* R_b D_s}{R} \quad (6)$$

220  $D_s$  represents the representative grain size. Specifically, I used the 84<sup>th</sup> percentile grain  
 221 size ( $D_{84}$ ) because coarser grains in a given grain size distribution posed a greater  
 222 influence on the channel morphology (MacKenzie et al., 2018; Shobe et al., 2021b).  $R_b$   
 223 denotes the relative buoyancy density of the sediment.

$$224 \quad R_b = \frac{\rho_s - \rho_w}{\rho_w}, \quad (7)$$

225 where  $\rho_s$  and  $\rho_w$  represent the densities of the sediment and water, respectively.  $R$   
 226 denotes the hydraulic radius, assuming a rectangular channel cross section.

$$227 \quad R = \frac{WH}{W + 2H}, \quad (8)$$

228 where  $H$  denotes the flow depth during the high-flow stage. The minimum and  
 229 maximum depths at each site were measured, and the mean value was used. The flow  
 230 depth at the time of the survey was measured using both a ruler and a laser  
 231 rangefinder. The width and depth near both the downstream and upstream ends of the  
 232 river sections where grain size was measured were documented. Details on how I  
 233 measured the grain size and density of gravel will be presented in subsequent  
 234 paragraphs.

235 The critical Shields number proposed by Lamb et al. (2008) is used.

$$236 \quad \tau_c^* = 0.15S^{\frac{1}{4}} \quad (9)$$

237  $\Delta S_{Q_s}$  is computed using an equation for bedload sediment transport proposed by  
238 Fernandez-Luque and van Beek (1976) (Sklar & Dietrich, 2006):

$$239 \quad \Delta S_{Q_s} = (\tau^* - \tau_c^*) \frac{R_b D_s}{R} \left( \frac{Q_s}{Q_c} \right)^{\frac{2}{3}} \quad (10)$$

240  $\frac{Q_s}{Q_c}$  represents the ratio of sediment supply to transport capacity (hereinafter, relative  
241 sediment supply). The relative sediment supply could not be measured in the field;  
242 thus, the ratio of exposed bedrock ( $F_e$ ) in the channel bed was used as a proxy  
243 (Chatanantavet and Parker, 2008).

$$244 \quad \frac{Q_s}{Q_c} = 1 - F_e \quad (11)$$

245  $F_e$  was recorded in the field as explained later. Subtracting the sum of  $S_{D_s}$  and  $\Delta S_{Q_s}$   
246 from the total slope yields  $\Delta S_E$  (Equation 4). Thereafter, each slope component was  
247 multiplied by upstream catchment area to the power of  $\theta_{ref}$  to obtain the three  
248 components of  $k_{sn}$  associated with  $S_{D_s}$ ,  $\Delta S_{Q_s}$ , and  $\Delta S_E$  (Lai et al., 2021):

$$249 \quad k_{sn} = (S_{D_s} + \Delta S_{Q_s} + \Delta S_E) A^{\theta_{ref}} = k_{sn}^{D_s} + k_{sn}^{Q_s} + k_{sn}^E \quad (12)$$

250 Wolman counting was employed to determine the grain size distributions. Intermediate  
251 axes of a minimum of 100 grains were measured from the surfaces of the gravel bars.  
252 To mitigate biases from inter- and intra-bar variability in grain size, gravel was sampled  
253 from multiple bars. The results represent the grain sizes of a river section extending at  
254 least 50 m along the stream. Additionally, the rock type of each grain was recorded to  
255 assess differences in grain size among rock types. Although several types of  
256 sedimentary and volcanic rocks were present, only two categories were used for  
257 simplicity: sedimentary and volcanic.

258 In the laboratory, the densities of these rock types were measured. In total, 51 grains  
259 of each type were collected, which exhibited densities of  $1.82 \times 10^3 \text{ kg/m}^3$  for  
260 sedimentary rocks and  $2.28 \times 10^3 \text{ kg/m}^3$  for volcanic rocks. Wolman counting indicated

261 that, on average, volcanic rock grains constituted 77% of the grains at each site.  
262 Consequently, a weighted average density ( $\rho_s$ ) of  $2.17 \times 10^3$  kg/m<sup>3</sup> was calculated based  
263 on the average abundance of each rock type at the channel bed.  
264 The degree of bedrock exposure on the riverbed ( $F_e$ ) was documented either visually or  
265 using an orthomosaic image, the latter being employed when the river channel was not  
266 obscured by vegetation. Owing to the narrow, vegetation-enclosed channels, using an  
267 unpiloted aerial vehicle was impractical. Instead, photographs were taken with a  
268 camera attached to a long pole, and the exposed bedrock areas were recorded on an  
269 iPad mini (6<sup>th</sup> generation, Apple Inc.). These images were then used to create an  
270 orthomosaic with AgiSoft Metashape software. The orthomosaic was imported into QGIS  
271 for  $F_e$  calculation. For visual estimates, an uncertainty of  $\pm 0.1$  was noted. In cases  
272 where no exposed bedrock was visible,  $F_e$  was assumed to be between 0 and 0.1, and a  
273 default value of 0.05 was used because of the difficulty of thoroughly inspecting the  
274 riverbed.

275

## 276 **4 RESULTS**

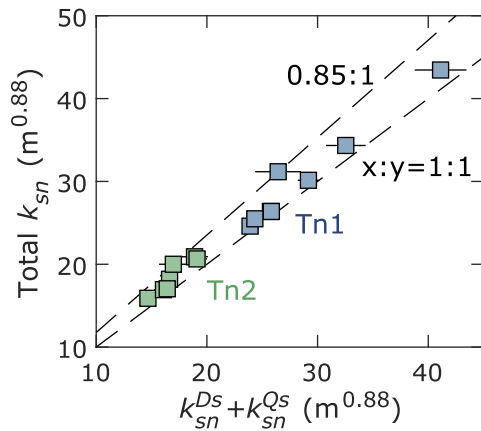
### 277 **4.1 Channel steepness in a catchment of single rock type**

278 The average  $k_{sn}$  values in the two Tanosawa channels (Tn1 and Tn2) were  $30 \text{ m}^{0.88}$  and  
279  $19 \text{ m}^{0.88}$ , respectively. (Figure. 3, Table 1). The average  $k_{sn}$  components related to  
280 sediment caliber,  $k_{sn}^{D_s}$  and  $k_{sn}^{Q_s}$ , were greater in Tn1 than in Tn2 by 3.7 and 7.9  $\text{m}^{0.88}$ ,  
281 respectively. In both streams, the sum of  $k_{sn}^{D_s}$  and  $k_{sn}^{Q_s}$  accounted for at least 85% of  
282 the total  $k_{sn}$  (Figure 4), indicating that the difference in  $k_{sn}$  between the two streams  
283 resulted from differences in  $k_{sn}^{D_s}$  and  $k_{sn}^{Q_s}$ .

284 Furthermore, I focused on the variables that caused the difference in  $k_{sn}^{D_s}$  and  $k_{sn}^{Q_s}$   
285 between Tn1 and Tn2. The average values for the three key parameters ( $R$ ,  $D_{84}$ , and  $F_e$ )

286 are listed in Table 1, which was used to evaluate  $S_{D_s}$  and  $\Delta S_{Q_s}$  (Equations 6 and 10).  
 287 The hydraulic radius  $R$  was 1.2 times greater in Tn1 than in Tn2, which reduced  $k_{sn}^{D_s}$   
 288 and  $k_{sn}^{Q_s}$  in Tn1 relative to those in Tn2. Wolman count was conducted at four and three  
 289 sites in Tn1 and Tn2, respectively. The resulting  $D_{84}$  was 1.4 times greater in Tn1 than  
 290 in Tn2. Given the uncertainty involved in estimating  $F_e$ ,  $F_e$  is almost similar or slightly  
 291 smaller for Tn1. As  $Q_c$  increases with the local channel slope, the similar bedrock  
 292 exposure in Tn1 and Tn2, despite the greater channel slope in Tn1, suggests that Tn1  
 293 was more strongly affected by the sediment load supplied upstream.

294



295

296 Figure 4. Comparison of  $k_{sn}$  associated with the imposed sediment load ( $k_{sn}^{D_s}$  and  $k_{sn}^{Q_s}$ )  
 297 and total  $k_{sn}$  in Tanosawa.

298

299 Table. 1. Channel and sediment characteristics in Tanosawa. The numbers except for  
 300  $D_{84}$  are average values over the studied section.

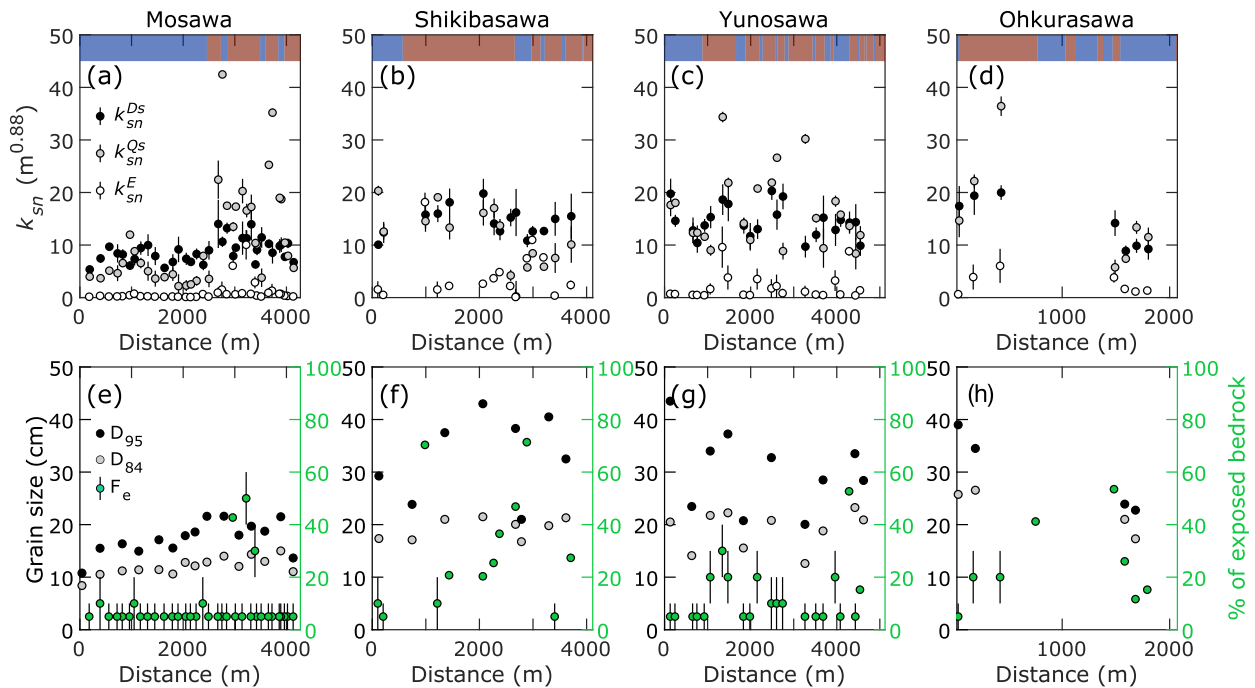
	$k_{sn}$ ( $m^{0.88}$ )	$k_{sn}^{D_s}$ ( $m^{0.88}$ )	$k_{sn}^{Q_s}$ ( $m^{0.88}$ )	R (m)	$D_{84}$ (cm)	$F_e$ (%)
Tn1	30.2	12.0	16.7	0.7	19	10.6
Tn2	18.5	8.3	8.7	0.6	14	20.3



301

## 302 4.2 Difference in $k_{sn}$ components between rock type

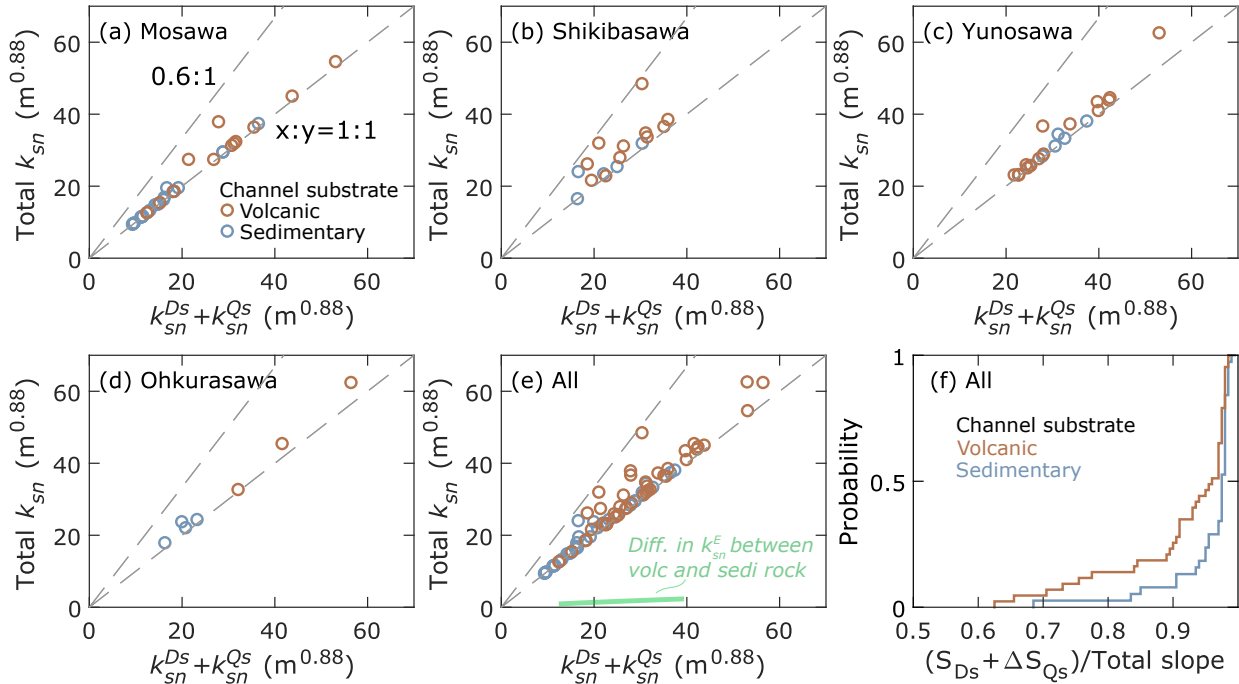
303 In Mosawa, the average  $k_{sn}$  was twice as high in volcanic rock reaches compared to  
304 sedimentary rock reaches (Figure 3b). A one-sided Wilcoxon rank-sum test confirmed  
305 that  $k_{sn}$  values were significantly higher in volcanic rock ( $p = 1.2 \times 10^{-4}$ ). The  
306 combined  $k_{sn}$  from the imposed sediment load ( $k_{sn}^{Ds}$  and  $k_{sn}^{Qs}$ ) accounted for 96% of the  
307 total  $k_{sn}$  on average, ranging from 85–99% in sedimentary rock reaches and 73–99%  
308 in volcanic rock reaches (Figures 5a, 6a). These findings suggest that variations in  $k_{sn}$   
309 were primarily caused by sediment effects.



310

311 Figure 5. Variation of each  $k_{sn}$  component and key factors associated with the imposed  
312 sediment load. The top bar in (a–d) represents channel substrate.

313



314

315 Figure 6. Comparison of  $k_{sn}$  associated with the imposed sediment load ( $k_{sn}^{Ds}$  and  $k_{sn}^{Qs}$ )

316 and total  $k_{sn}$  for volcanic and sedimentary rock. (e) Results of four rivers. Thin green

317 line at the bottom represents the difference in total  $k_{sn}$  between rock types predicted

318 by the tentative regression analysis. Refer to the main text for the details. (f)

319 Cumulative distribution function of the ratio of slope component associated with the

320 sediment load and total slope.

321

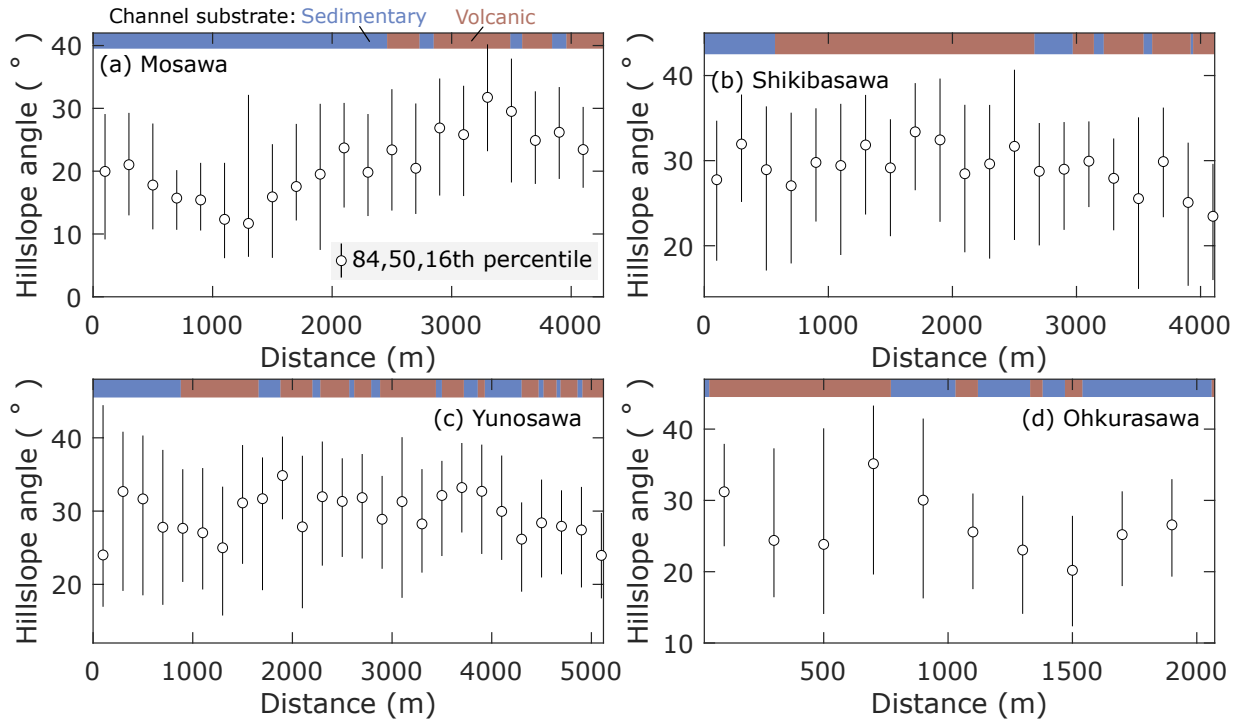
322 In Mosawa, grain size did not significantly change in the most upstream section but

323 began to decrease downstream near the lithologic boundary at 2460 m (Figure 5e). The

324 hillslope angles were considerably steeper in the upstream section underlain by basaltic

325 rock compared to the downstream section (Figure 7a).

326



327

328 Figure 7. Angles of hillslopes along the trunk stream in each river catchment. The top

329 bar represents channel substrate.

330

331 In Shikibasawa, the average  $k_{sn}$  in volcanic rock reaches was 1.3 times larger than that

332 in the sedimentary rock reaches (Figure 3c). A one-sided Wilcoxon rank-sum test also

333 confirmed significantly higher  $k_{sn}$  values in volcanic rock reaches ( $p = 1.2 \times 10^{-2}$ ) at a

334 5% significance level. In the most upstream section, where sedimentary rock layers

335 occurred intermittently,  $k_{sn}$  values did not exhibit clear variation with the rock type

336 (Figure 3c). However, downstream from 2660 m, the  $k_{sn}$  values increased and then

337 decreased at 600 m, coinciding with a transition from volcanic to sedimentary rock

338 (Figure 3c). The sum of  $k_{sn}^{Ds}$  and  $k_{sn}^{Qs}$  accounted for 87% of the total  $k_{sn}$  on average,

339 with 69–99% in sedimentary rock reaches and 63–98% in volcanic rock reaches

340 (Figures 5b, 6b).

341 In Shikibasawa, although the  $D_{84}$  did not systematically decrease across the studied  
342 sections, the 95th percentile grain size ( $D_{95}$ ) downstream from 570 m was significantly  
343 smaller than upstream values. This reduction in  $D_{95}$  corresponded with the bedrock  
344 transition from volcanic to sedimentary rocks. Regarding bedrock exposure ( $F_e$ ), despite  
345 significant local variations rendering it difficult to discern a general trend, bedrock was  
346 more extensively exposed in the upstream reaches (distance > 600 m) dominated by  
347 volcanic rock than in the most downstream reaches underlain by sedimentary rock. The  
348 hillslope angles increased slightly downstream in the headwaters (distance > 3000 m)  
349 and remained relatively constant throughout the studied section (Figure 7b).

350 In Yunosawa, the local variation in  $k_{sn}$  was large and did not correspond to the changes  
351 in the bedrock (Figure 3d). The volcanic and sedimentary rock reaches exhibited similar  
352  $k_{sn}$  values that were indistinguishable in a two-sided Wilcoxon rank-sum test ( $p =$   
353 0.86). The mean ratio of the sum of  $k_{sn}^{Ds}$  and  $k_{sn}^{Qs}$  to total  $k_{sn}$  was 95% for all the data.  
354  $k_{sn}^{Ds}$  and  $k_{sn}^{Qs}$  occupied 91–98% of total  $k_{sn}$  in the reaches of sedimentary rock and 76–  
355 98% in the reaches of volcanic rock (Figures. 5c, 6c).

356 The grain size in Yunosawa varied widely over short distances and did not follow a  
357 systematic trend as predicted by Sternberg's law (Figure 5g). The hillslope angles were  
358 consistent across the studied sections (Figure 7c). Although observations of  $F_e$  were  
359 limited, the bedrock was relatively well-exposed in an area between approximately  
360 1000–1500 m, which roughly corresponded to the section with a higher  $k_{sn}$  (1250–  
361 1600 m in distance) compared to neighboring sections (Figures 3d and 5g).

362 In Ohkurasawa, although  $k_{sn}$  did not vary markedly upstream from 800 m, it started to  
363 increase downstream at 800 m, where the channel substrate changed from  
364 sedimentary to volcanic (Figure 3e). The average  $k_{sn}$  is 26.1 and 50  $m^{0.88}$  for the  
365 sedimentary and volcanic rock, respectively. The difference in  $k_{sn}$  between rock types

366 was significant in a one-sided Wilcoxon rank-sum test ( $p = 6.3 \times 10^{-3}$ ). The sum of  $k_{sn}^{D_s}$   
367 and  $k_{sn}^{Q_s}$  accounted for 92% of total  $k_{sn}$  on average, 84–95% for reaches of  
368 sedimentary rock, and 90–98% for reaches of volcanic rock (Figures 5d, 6d).

369 The grain size was significantly larger in the steeper downstream section compared to  
370 the gentler upstream section (Figure 5h). The hillslope angles also increased  
371 downstream near the lithologic boundary at approximately 1000 m, where volcanic rock  
372 began to outcrop in the upper parts of the hillslopes (Figures 1d and 7d). The upstream  
373 of this lithologic boundary, the hillslope angles did not exhibit clear variations with the  
374 rock type.

375 Overall, the sum of  $k_{sn}^{D_s}$  and  $k_{sn}^{Q_s}$  accounted for 94% of total  $k_{sn}$  on average, indicating  
376 that the effects of the imposed sediment load could mostly explain the variation in total  
377  $k_{sn}$  (Figure 6e). Figure 6f displays the cumulative histogram of the ratio of  $S_{D_s} + \Delta S_{Q_s}$   
378 ( $k_{sn}^{D_s} + k_{sn}^{Q_s}$ ) to total slope ( $k_{sn}$ ) for sedimentary and volcanic rock. The effects of the  
379 sediment load explain a smaller fraction of the total  $k_{sn}$  for the reaches of volcanic rock  
380 than that for the reaches of sedimentary rock. The difference in the fraction of  $S_{D_s} + \Delta S_{Q_s}$   
381 between the rock type is significant in a one-sided Wilcoxon ranksum test ( $p = 1.6 \times$   
382  $10^{-3}$ ; null hypothesis: the fraction of  $S_{D_s} + \Delta S_{Q_s}$  is smaller for the reaches of sedimentary  
383 rock than those of the volcanic rock). To quantify the difference in  $k_{sn}^E$  between the two  
384 rock types, I performed a regression analysis of  $k_{sn}^{D_s} + k_{sn}^{Q_s}$  and the total  $k_{sn}$  and  
385 calculated the difference between the predicted total  $k_{sn}$  of the volcanic and  
386 sedimentary rocks. We assumed an exponential relationship because it yielded a higher  
387  $R^2$  value than linear and power relationships. The resulting difference in the predicted  
388 total  $k_{sn}$  values was  $0.9\text{--}2.3 \text{ m}^{0.88}$  (green line in Figure 6e), which is 5–7% of the  
389 predicted total  $k_{sn}$  for volcanic rock. This result signifies that when the impact of the  
390 imposed sediment load on total  $k_{sn}$  is the same between rock types, total  $k_{sn}$  in

391 volcanic rock is only 5–7% greater than  $k_{sn}$  in sedimentary rock. However, if I consider  
392 the difference between the maximum and minimum bounds of the 95% prediction  
393 intervals of the predicted total  $k_{sn}$  for volcanic and sedimentary rocks, i.e. the  
394 maximum difference in the predicted  $k_{sn}^E$  between rock types, the difference in total  $k_{sn}$   
395 becomes 26–53% of the total  $k_{sn}$  for volcanic rock.

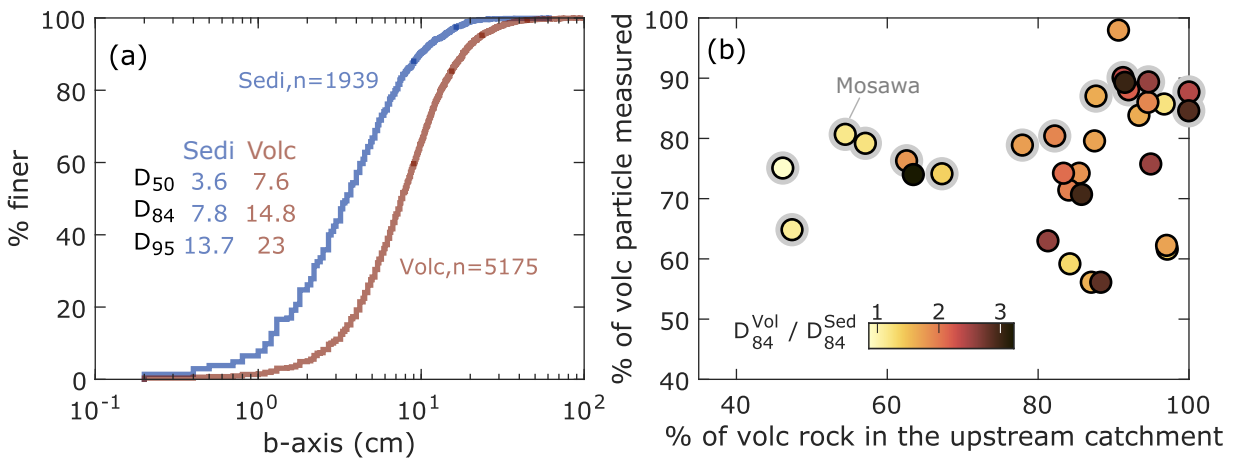
396

### 397 **4.3 Size and composition of bed materials**

398 This section examines the variation in grain size and the proportion of specific rock  
399 particles across different sites. Among the 7,114 grains collected, 73% were of volcanic  
400 origin. The median grain size ( $D_{50}$ ) of volcanic rocks was 2.1 times larger than that of  
401 sedimentary rocks (Figure 8a). The  $D_{50}$  ratio between volcanic and sedimentary rocks  
402 varied across the four rivers studied—Mosawa, Shikibasawa, Yunosawa, and  
403 Ohkurasawa—with values ranging from 1.9 to 3.2 (Supporting Information Figure S2).  
404 Similarly, the  $D_{84}$  and  $D_{95}$  of volcanic rocks were larger than those of sedimentary rocks,  
405 and the magnitude of the difference between the rock types varied across the four  
406 rivers (Figures 8a and Supporting Information Figure S2). This variation suggests that  
407 the initial grain size distributions, which are supplied from hillslopes to channels, differs  
408 from one basin to another.

409 To explore the impact of changes in sediment source on bed material composition, the  
410 proportion of volcanic particles in each Wolman count was calculated and compared  
411 with the proportion of volcanic rock units within the catchment area at each site (Figure  
412 8b). The colors of the points in Figure 8b represent the ratio of the  $D_{84}$  for the volcanic  
413 and sedimentary rock particles ( $D_{84}^{Vol}$  and  $D_{84}^{Sed}$ , respectively). Despite the sampling  
414 biases associated with the Wolman count method (Bunte & Abt, 2001), which typically  
415 favor the selection of larger particles, the proportion of volcanic particles did not

416 correlate with  $D_{84}^{Vol}/D_{84}^{Sed}$  (Figure 8b). This suggests that sampling biases had minimal  
 417 impact on the results. In the Mosawa River, where basaltic rocks occur only in the  
 418 upstream half of the catchment (Figure 3), the proportion of basaltic particles in the  
 419 riverbed decreases downstream as the basaltic rock units occupy a smaller area of the  
 420 catchment (grey circles in Figure 8b).  
 421 Despite this, the proportion of basaltic particles remains above 64% even when basaltic  
 422 rock constitutes only 45% of the upstream area, indicating an overrepresentation of  
 423 basaltic gravel in the riverbed. In contrast, in the other three rivers where volcanic and  
 424 sedimentary rocks are interspersed throughout the studied reach, no clear correlation  
 425 was observed between the proportion of volcanic grains in the riverbed and in the  
 426 catchment area, potentially because of the intermittent supply of volcanic rock .  
 427



428  
 429 Figure 8. (a) Cumulative frequency of b-axis for particles of sedimentary and volcanic  
 430 rock. (b) Effect of changing sediment source on the proportion of volcanic particles at  
 431 the channel bed. The color indicates the ratio of the 84th percentile grain size for the  
 432 volcanic and sedimentary rock particles measured in each Wolman count. Gray circles  
 433 are data in Mosawa.

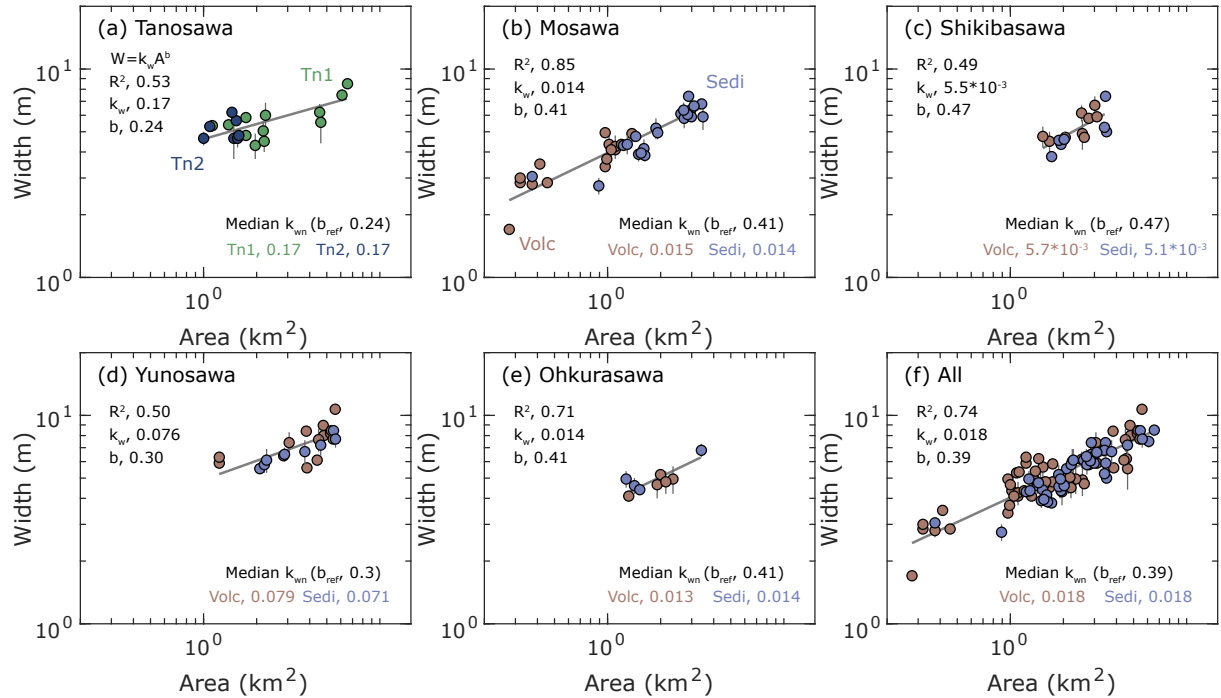
434

#### 435 **4.4 Dependency of channel width on rock type**

436 Figure 9 presents the channel widths measured at 102 sites alongside the results of the  
437 regression analysis (Equation 3). Across all rivers, a gradual increase in channel width  
438 with drainage area was observed. The exponent  $b$  in Equation 3 varied from 0.24 to  
439 0.47 across individual rivers, with an overall value of 0.39 for the entire dataset, a  
440 typical value for mountain streams (Montgomery & Gran, 2001). In Tanosawa, despite  
441 larger grain sizes and higher  $k_{sn}$  values in the trunk stream Tn1 compared to the  
442 tributary Tn2, the  $k_{wn}$  values were statistically similar between Tn1 and Tn2 as  
443 indicated by the two-sided Wilcoxon rank-sum test (Figure 9a,  $p = 0.54$ ). In Mosawa  
444 and Shikibasawa, the median  $k_{wn}$  was slightly higher in volcanic rock reaches than in  
445 sedimentary rock reaches (Figures 9b and 9c); however, these differences were not  
446 statistically significant at the 5% level, even with a one-sided Wilcoxon rank-sum test  
447 ( $p = 0.06$  for both Mosawa and Shikibasawa; the null hypothesis being that  $k_{wn}$  is  
448 smaller for volcanic rock reaches than for sedimentary rock reaches).

449 The median  $k_{wn}$  in Yunosawa was significantly larger for volcanic rock reaches than for  
450 sedimentary rock reaches ( $p = 0.028$  in the two-sided Wilcoxon rank-sum test) (Figure  
451 9d). Conversely, in Ohkurasawa, the median  $k_{wn}$  was significantly larger for  
452 sedimentary rock reaches than for volcanic rock reaches ( $p = 0.032$  in the two-sided  
453 Wilcoxon rank-sum test) (Figure 9e). Overall, no significant differences in  $k_{wn}$  between  
454 volcanic and sedimentary rocks were found in the two-sided Wilcoxon rank-sum test ( $p$   
455 = 0.12), suggesting that factors other than rock strength influence channel width.





456

457 Figure 9. (a–e) Variation of channel width in each river and (f) whole study area. The  
 458 numbers at the top left and the gray line show the results of curve fitting and the  
 459 predicted width, respectively. Circles in (b–f) are colored by channel substrate.

460

## 461 5 Discussion

### 462 5.1 Quantifying the impact of sediment on stream profiles in mono- 463 lithologic catchment

464 The analysis revealed that the difference in total  $k_{sn}$  between Tn1 and Tn2 in Tanosawa  
 465 corresponded to the differences in  $k_{sn}^{Ds}$  and  $k_{sn}^{Qs}$  (Table 1). Given their proximity of only  
 466 a few hundred meters, it is likely that Tn1 and Tn2 experienced similar climatic and  
 467 tectonic forces, aligning with the observation that variations in  $k_{sn}$  predominantly  
 468 resulted from sediment impacts. Although the possibility that rock erodibility  
 469 significantly differs between Tn1 and Tn2 due to heterogeneous macro- and microscopic  
 470 rock properties cannot be entirely ruled out (e.g., Turowski et al., 2023), the major

471 cause of the contrasting profiles between Tn1 and Tn2 is argued to be the difference in  
472 grain size, as they exhibit similar  $k_{wn}$  values and hillslope angles, which are also  
473 influenced by rock properties (Allen et al., 2013; Roda-Boluda et al., 2018). These  
474 findings in Tanosawa support the observations in the other four streams that sediment  
475 load significantly contributes to the total  $k_{sn}$  (Figures 6e, 6f).

476 The results of Tanosawa highlight the significance of acknowledging the spatial  
477 heterogeneity of rock properties within a geological unit and its impact on the grain size  
478 distribution in channels. Basaltic gravel constitutes 83–97% of the total gravel  
479 measured in Tanosawa, suggesting that the differences in grain size between Tn1 and  
480 Tn2 can be attributed to the initial grain size distribution of basaltic rock on hillslopes.  
481 Basaltic rocks in Tanosawa appear in various forms, including outcrops with sparse or  
482 dense joints and severe spheroidal weathering (Tsushima & Uemura, 1959; Uemura et  
483 al., 1959).

484 Although vegetation cover limited detailed observations of the bedrock outcrops, the  
485 heterogeneity of rock properties probably caused the differences in grain size between  
486 Tn1 and Tn2. The sizes of volcanic gravel in four other streams also varied significantly  
487 (Supporting Information Figure S2), implying that the local changes in the size of  
488 volcanic gravel induced by varying degrees of fracturing, weathering, and mass  
489 movement are common in this area. Although numerous studies including the present  
490 research demonstrate that the imposed sediment load rather than rock strength  
491 controls the morphology of mountain rivers, the findings of this study confirm that it is  
492 important to reveal how rock properties dictate the size and rates of sediment supply  
493 into channels (Sklar et al., 2017).

494

## 495 **5.2 Relative importance of rock erodibility and sediment load on** 496 **setting channel slope**

497 This section initially addresses the transient response to the uplift of Tsugaru Mountain  
498 and the variation in channel width between rock types that potentially contribute to the  
499 observed variation in  $k_{sn}$ . It then examines how the substrate rock type influences  
500 longitudinal channel profiles.

501 The uplift of Tsugaru Mountain, initiated in the late Pliocene due to the activity of the  
502 Tsugaru fault (Nemoto, 2014), has not been precisely dated. However, the five streams  
503 studied may still be in a transient state, as adjustments to changes in base-level fall  
504 rates can take millions of years (Whittaker et al., 2007; Yanites, 2018; Takahashi et al.,  
505 2023). A sustained increase in the rate of base-level change can create a knickpoint  
506 that propagates upstream, dividing the stream into a steeper downstream section and a  
507 gentler upstream section. After the knickpoint passes, changes in channel width ( $k_{wn}$ )  
508 and the angles of adjacent hillslopes may occur (Whittaker et al., 2007; Hurst et al.,  
509 2012; Yanites, 2018; Baynes et al., 2022; Takahashi et al., 2023). Despite the  
510 presence of numerous knickpoints in the studied catchment, they do not correspond  
511 with changes in the reach average  $k_{sn}$  or systematic alterations in hillslope angles and  
512  $k_{wn}$  (Figures 3, 7, and 9). Therefore, it can be concluded that the transient response to  
513 changes in uplift rates has a negligible effect on  $k_{sn}$ .

514 Thereafter, I examined whether the difference in  $k_{wn}$  between the rock types affected  
515 the variations in  $k_{sn}$ . Although the reaches of volcanic and sedimentary rocks exhibited  
516 similar  $k_{wn}$  values in Tanosawa, Mosawa, and Shikibasawa, the reaches of volcanic rock  
517 displayed marginally larger  $k_{wn}$  values in Yunosawa and smaller  $k_{wn}$  values in  
518 Ohkurasawa than those of sedimentary rock (Figure 9). Generally, wider channels  
519 require steeper slopes than narrower channels to achieve equivalent incision rates.

520 Therefore, the differences in  $k_{wn}$  between rock types in Yunosawa and Ohkurasawa  
521 might have influenced the observed  $k_{sn}$  values. Nonetheless, since the difference in  
522 channel width between rock types is accounted for in the slope component calculations  
523 (Equations 6 and 10) and the median  $k_{wn}$  varies by only 10% between rock types,  
524 omitting the channel width difference does not alter the interpretation of how rock  
525 erodibility and sediment load impact channel slope.

526 Subsequently, I explored how substrate rock type influences channel morphology  
527 through its erodibility and the supply of coarse sediment. The slope components related  
528 to the imposed sediment load predominantly explain the variation in channel slope. The  
529 proportion of the residual component,  $\Delta S_E$ , averages 3% and ranges from 1% to 38%.  
530 This proportion of  $\Delta S_E$  is generally higher in volcanic rock reaches than in sedimentary  
531 rock reaches (Figure 6f). This disparity in  $\Delta S_E$  between the rock types can be attributed  
532 to the differential rock erodibility, as climate, tectonics, and  $k_{wn}$  do not account for the  
533 variation in  $\Delta S_E$ . Despite potential large uncertainties, the regression analysis revealed  
534 that the difference in  $k_{sn}^E$  between rock types amounts to only 5–7% of the predicted  
535  $k_{sn}$  for volcanic rock (Figure 6e). Even in an extreme case scenario that used the 95%  
536 prediction interval, the difference in  $k_{sn}^E$  between rock types ranged from a quarter to  
537 half of the predicted  $k_{sn}$  for volcanic rock. Thus, the influence of rock erodibility is  
538 considerably smaller than that of the imposed sediment load, which is consistent with  
539 the predictions from theoretical models (Sklar & Dietrich, 2006; Turowski et al., 2007).

540 The major influence of the sediment load on channel slope relative to rock erodibility  
541 suggests that the capacity of rock to supply coarse and immobile materials into  
542 channels determines the shape of longitudinal profiles. Sediment particles from hard  
543 rocks are typically coarser (Roda-Boluda et al., 2018), exhibit lower mass loss rates  
544 during transport (Attal & Lavé, 2009; Bodek & Jerolmack, 2021), and are denser than

545 those from soft rocks (Turowski et al., 2023). These characteristics contribute to the  
546 selective deposition and extended residence time of particles from harder rocks  
547 compared to those from softer rocks, as suggested by the disproportionate presence of  
548 volcanic gravel in the bed relative to the areal extent of volcanic rock in the catchment  
549 (Figure 8b). Consequently, the impact of sediment load can persist even when the  
550 bedrock transitions downstream from harder to softer types, thereby diminishing the  
551 disparity in channel steepness between different rock types (Johnson et al., 2009;  
552 Thaler and Covington, 2016; Finnegan et al., 2017; Lai et al., 2021). Thus,  
553 understanding the relationship between channel steepness and rock type necessitates  
554 an examination of how rock properties influence the sediment size supplied to channels  
555 (Sklar et al., 2017).

556 The predominant role of sediment load in determining channel slope complicates the  
557 assessment of a uniform response among mountain rivers in a region to changes in  
558 lithology and external conditions. Local factors such as proximity to tributary junctions,  
559 bedrock exposure along channels (Rice, 1998; Rice & Church, 1998), and  
560 heterogeneous rock properties influence the grain size distributions of bed material  
561 (DiBiase et al., 2018b; Verdian et al., 2021). The downstream evolution of grain size  
562 does not always follow the simple model (e.g., Sternberg's law) because of varied  
563 sediment sources and the mixing of rocks with different durability (Rice & Church,  
564 1998; Attal & Lavé, 2006). Moreover, sediment dynamics can impact channel width  
565 (MacKenzie & Eaton, 2017), potentially causing alterations in channel slope (Yanites,  
566 2018). Therefore, it is reasonable to expect variations in the differences in  $k_{sn}$  and  $k_{wn}$   
567 between rock types from one catchment to another on Tsugaru Mountain, where the  
568 disparity in grain size between rock types varied between catchments (Supporting  
569 Information Figure S2).

570 The dominance of either the tool or cover effect of sediment on erosion may dictate  
571 channel responses to changes in rock type. The erosional efficiency is influenced by the  
572 relative sediment supply (Sklar & Dietrich, 2001; Cowie et al., 2008; Scheingross et al.,  
573 2014). In a case of low relative sediment supply (tool regime), an increase in sediment  
574 supply accelerates erosion. Conversely, in a case of high relative sediment supply  
575 (cover regime), an increase in sediment supply inhibits erosion. Therefore, when a  
576 transition in rock type coincides with an increased sediment supply in the tool regime,  
577 the rivers can maintain similar erosion rates while reducing their channel slope from its  
578 original value (Sklar & Dietrich, 2004). In the cover regime, however, the channel slope  
579 must increase to counteract the increased sediment supply resulting from changes in  
580 rock type and maintain similar erosion rates across lithologic boundaries. Additionally,  
581 the temporal variations in the channel slope caused by the knickpoint passage or  
582 damming via slope failure may locally shift a reach from the cover to the tool regime or  
583 vice versa, thereby complicating the interpretation of how rock type influences channel  
584 slope. Although testing these hypotheses was beyond the scope of this study, future  
585 laboratory and numerical experiments could explore how rivers in the tool and cover  
586 regimes respond to variations in rock erodibility and sediment supply.

587 Although the channel slope is typically influenced by sediment load, the variations in  
588 rock erodibility between the rock types are evident in the study area. Waterfalls  
589 predominantly occur in volcanic rock reaches and near lithologic boundaries (Figure 3).  
590 These local highs of  $k_{sn}$  are probably attributable to low rock erodibility, as bedrock  
591 exposure is more extensive in these steep reaches compared to adjacent gentler areas.  
592 This observation is supported by the model predictions of Guryan et al. (2024), who  
593 employed a modified version of the stream power model incorporating the conservation  
594 and transport of eroded mass (Shobe et al., 2017). Their analysis of river profiles

595 incising layered rock revealed that higher channel slopes in hard rock, relative to soft  
596 rock, caused by the differences in rock erodibility, lead to greater sediment entrainment  
597 rates in hard rock reaches. Consequently, this results in a thinner sediment cover in  
598 areas of hard rock.

599 The results of Guryan et al. (2024) align with observations in Tsugaru; however, it is  
600 important to note that the thinning of the alluvial cover discussed occurs when the  
601 sediment supply remains relatively constant (Guryan et al., 2024). As such, significant  
602 differences in the size and quantity of sediment from adjacent hillslopes with rock type  
603 can negate the effects of increased entrainment rates and lead to thicker alluvial cover  
604 in areas with hard rock. In Tsugaru, the observed local increases in  $k_{sn}$  did not  
605 correspond to the abrupt changes in hillslope angles or tributary junctions, indicating  
606 minor variations in sediment supply. Investigating these steeper reaches with thinner  
607 alluvial cover could reveal the conditions under which the influence of rock erodibility on  
608 channel slope outweighs that of the imposed sediment load. However, studying such  
609 steep reaches was impractical, as they were exceedingly steep to traverse for several  
610 hundred meters along the channel and lacked numerous subaerial bars necessary for  
611 measuring more than 100 grains.

612 The variation in rock layers with differing erodibilities may have also contributed to the  
613 apparent decorrelation of rock erodibility and the channel slope in Tsugaru. When  
614 bedrock incision rates are highly dependent on rock erodibility, as seen under the  
615 detachment-limited condition in the stream power model (Whipple & Tucker, 1999),  
616 differential incision across each rock unit modifies the rates of local base-level change  
617 at their interfaces (Forte et al., 2016; Perne et al., 2017). This local base-level change  
618 can lead to a steeper channel slope or slower incision in softer rocks compared to  
619 harder rocks (Forte et al., 2016; Perne et al., 2017). In Tsugaru, volcanic rock intrudes

620 into sedimentary rock, forming sills of varying thicknesses parallel to the bedding of the  
621 sedimentary rock (Tsushima & Uemura, 1959; Uemura et al., 1959). The stratified  
622 structure was most evident at Yunosawa, where the substrate rock alternated  
623 frequently within the middle of the studied reach (Figures 1d and 3d). Unlike the four  
624 other rivers studied,  $k_{sn}$  values in the volcanic and sedimentary rocks at Yunosawa  
625 were statistically indistinguishable, potentially because of the local base-level changes  
626 caused by differential incision in the volcanic and sedimentary rocks.

627

### 628 **5.3 Limitations in the slope component analysis**

629 Slope component analysis is a valuable method for quantifying the contributions of  
630 imposed sediment load to longitudinal stream profiles using field-measurable  
631 parameters (Sklar & Dietrich, 2006; Lai et al., 2021). However, certain parameters  
632 required for this analysis are not easily measurable in the field and depend on the  
633 selection of theoretical or empirical equations. In this discussion, I address the  
634 challenges in calculating  $S_{D_s}$  and  $\Delta S_{Q_s}$  and provide their minimum estimates.

635 A primary concern is the entrainment threshold,  $\tau_c^*$ . We adopted  $\tau_c^*$  proposed by Lamb  
636 et al. (2008), which is a simple function of channel slope. This threshold is practical for  
637 field studies and is applicable to headwater streams, as it is derived from both flume  
638 and field data encompassing a channel slope up to 0.2, typical of headwaters.

639 Nonetheless, accurate estimation of  $\tau_c^*$  has proven extremely challenging (Buffington &  
640 Montgomery, 1997; Petit et al., 2015; Phillips et al., 2022; Perret et al., 2023; Hodge  
641 et al., 2024). Among the various factors causing spatial and temporal variations in  $\tau_c^*$ ,  
642 grain protrusion is arguably the most significant when calculating the slope component  
643 related to the entrainment threshold ( $S_{D_s}$ ). Coarser grains in a given grain size  
644 distribution tend to protrude from the bed, exposing a larger area to the flow. This



645 modifies  $\tau_c^*$  based on the protruded height of the grain relative to  $D_{50}$  (Hodge et al.,  
646 2019; Smith et al., 2023), significantly reducing  $\tau_c^*$  for grains sized  $D_{84}$  compared to the  
647 value predicted by Equation 9, which is based on the median-sized grains (Lamb et al.,  
648 2008).

649 Despite these complexities, I argue that the slope component  $S_{D_s}$  remains critical  
650 because the residence time of gravel in the channel is influenced by both the frequency  
651 of entrainment and the transport distance. Vázquez-Tarrío et al. (2019) and Liébault et  
652 al. (2023) have compiled published data on gravel transport using passive and active  
653 tracers, respectively. Their findings reveal that the transport distance of gravel  
654 decreases exponentially with size relative to the median grain size. Furthermore, once a  
655 large grain on the bar is entrained, the bed roughness decreases, and the grains  
656 previously sheltered by the entrained grain become more mobile. Therefore, although  
657 estimates of  $S_{D_s}$  may vary significantly when accounting for grain protrusion, the  
658 impact is mitigated by the exponential reduction in transport distance with size and the  
659 reorganization of the bed following the entrainment of coarse grains.

660 Quantifying the relative sediment supply  $\frac{Q_s}{Q_c}$  from the areal fraction of exposed bedrock  
661  $F_e$  (Equation 11) presents a significant challenge. Flume experiments conducted by  
662 Chatanantavet and Parker (2008) demonstrated that  $F_e$  either linearly decreases with  
663 an increase in the relative sediment supply or abruptly dropped from 1 (fully exposed)  
664 to 0 (no exposure). Subsequent studies confirmed both gradual and abrupt alluviation  
665 (Johnson & Whipple, 2010; Inoue et al., 2014; Mishra & Inoue, 2020; Cho & Nelson,  
666 2024), and the rate of change in  $F_e$  with the increasing relative sediment supply is  
667 much more diverse than predicted by Equation 11, partly due to the relative surface  
668 roughness of the alluvial cover and bedrock (Mishra & Inoue, 2020). However, owing to

669 the lack of constraints on the roughness of the bedrock, discussing the uncertainty in  
670 the relative sediment supply calculated in Tsugaru is not feasible.  
671 The difficulties with accurate constraints on  $S_{D_s}$  and  $\Delta S_{Q_s}$  indicate that their minimum  
672 estimates can be presented to ensure the validity of the present findings. For  $S_{D_s}$ , I  
673 used  $\tau_c^* = 0.02$ , which is roughly one-third of the values predicted by Lamb et al. (2008)  
674 and in the smallest range reported in previous studies (Buffington & Montgomery,  
675 1997; Petit et al., 2015; Perret et al., 2023). For  $\Delta S_{Q_s}$ , I set  $F_e = 0.7$  for all sites, the  
676 minimum value observed in Tsugaru (Figure 5) and used  $\frac{Q_s}{Q_c} = 0.3$ , which is generally  
677 lower than the values predicted by the existing models (Mishra & Inoue, 2020). Except  
678 for  $\tau_c^*$  and  $\frac{Q_s}{Q_c}$ , I used the same parameters as those used to calculate  $S_{D_s}$  and  $\Delta S_{Q_s}$   
679 displayed in Figure 5. The resulting sum of  $S_{D_s}$  and  $\Delta S_{Q_s}$  occupies 47–64% of total  
680 slope, which is approximately 57% of the values on average presented in Figure 6f.  
681 Therefore, I can reasonably conclude that the imposed sediment load controls the  
682 channel slope more strongly than rock erodibility.

683

## 684 **6 Conclusions**

685 The minimum channel slope required to transport the imposed sediment load for five  
686 rivers in the Tsugaru Mountain region were calculated to determine that the sediment  
687 load generally exerts a stronger influence on channel slope than rock erodibility. This  
688 finding persists even when using very small values for the threshold of incipient motion  
689 and relative sediment supply to estimate sediment effects. Additionally, the locally  
690 steepened reaches with the thinner alluvial cover possibly resulted from contrasts in  
691 erodibility, which is consistent with previous model predictions. These observations  
692 confirm that rock strength influences stream profiles by modulating erosional resistance

693 and the mobility of rock particles. They suggest that future studies should investigate  
694 the conditions under which the effects of rock erodibility outweigh the impact of  
695 sediment load. The slope component analysis facilitates the quantification of sediment  
696 impact, which is challenging to estimate in the field. However, it is important to  
697 acknowledge that the uncertainty in the results could not be evaluated easily due to  
698 difficulties in constraining the entrainment threshold and relative sediment supply.

699

## 700 **REFERENCES**

701 Allen, G. H., Barnes, J. B., Pavelsky, T. M., & Kirby, E. (2013). Lithologic and  
702 tectonic controls on bedrock channel form at the northwest Himalayan  
703 front. *Journal of Geophysical Research: Earth Surface*, *118*(3), 1806–  
704 1825. <https://doi.org/10.1002/jgrf.20113>

705 Anderson, S., Gasparini, N., & Johnson, J. (2023). Building a bimodal  
706 landscape: Bedrock lithology and bed thickness controls on the  
707 morphology of Last Chance Canyon, New Mexico, USA. *Earth Surface  
708 Dynamics*, *11*(5), 995–1011. [https://doi.org/10.5194/esurf-11-995-  
709 2023](https://doi.org/10.5194/esurf-11-995-2023)

710 Attal, M., & Lavé, J. (2006). Changes of bedload characteristics along the  
711 Marsyandi River (central Nepal): Implications for understanding hillslope  
712 sediment supply, sediment load evolution along fluvial networks, and  
713 denudation in active orogenic belts. In S. D. Willett, N. Hovius, M. T.  
714 Brandon, & D. M. Fisher, *Tectonics, Climate, and Landscape Evolution*.  
715 Geological Society of America. [https://doi.org/10.1130/2006.2398\(09\)](https://doi.org/10.1130/2006.2398(09))

716 Attal, M., & Lavé, J. (2009). Pebble abrasion during fluvial transport:  
717 Experimental results and implications for the evolution of the sediment  
718 load along rivers. *Journal of Geophysical Research: Earth Surface*,  
719 *114*(F4), 2009JF001328. <https://doi.org/10.1029/2009JF001328>

720 Baynes, E. R. C., Lague, D., Steer, P., & Davy, P. (2022). Dynamic bedrock  
721 channel width during knickpoint retreat enhances undercutting of  
722 coupled hillslopes. *Earth Surface Processes and Landforms*, *47*(15),  
723 3629–3640. <https://doi.org/10.1002/esp.5477>

724 Bodek, S., & Jerolmack, D. J. (2021). Breaking down chipping and  
725 fragmentation in sediment transport: The control of material strength.  
726 *Earth Surface Dynamics*, *9*(6), 1531–1543.  
727 <https://doi.org/10.5194/esurf-9-1531-2021>

728 Buffington, J. M., & Montgomery, D. R. (1997). A systematic analysis of  
729 eight decades of incipient motion studies, with special reference to  
730 gravel-bedded rivers. *Water Resources Research*, *33*(8), 1993–2029.  
731 <https://doi.org/10.1029/96WR03190>

732 Bursztyn, N., Pederson, J. L., Tressler, C., Mackley, R. D., & Mitchell, K. J.  
733 (2015). Rock strength along a fluvial transect of the Colorado Plateau –  
734 quantifying a fundamental control on geomorphology. *Earth and*  
735 *Planetary Science Letters*, *429*, 90–100.  
736 <https://doi.org/10.1016/j.epsl.2015.07.042>

737 Carr, J. C., DiBiase, R. A., Yeh, E.-C., Fisher, D. M., & Kirby, E. (2023). Rock  
738 properties and sediment caliber govern bedrock river morphology across  
739 the Taiwan Central Range. *Science Advances*, 9(46), eadg6794.  
740 <https://doi.org/10.1126/sciadv.adg6794>

741 Chatanantavet, P., & Parker, G. (2008). Experimental study of bedrock  
742 channel alluviation under varied sediment supply and hydraulic  
743 conditions. *Water Resources Research*, 44(12), 2007WR006581.  
744 <https://doi.org/10.1029/2007WR006581>

745 Cho, J., & Nelson, P. A. (2024). Patterns of Alluviation in Mixed Bedrock-  
746 Alluvial Channels: 2. Controls on the Formation of Alluvial Patches.  
747 *Journal of Geophysical Research: Earth Surface*, 129(1),  
748 e2023JF007293. <https://doi.org/10.1029/2023JF007293>

749 Cowie, P. A., Whittaker, A. C., Attal, M., Roberts, G., Tucker, G. E., & Ganas,  
750 A. (2008). New constraints on sediment-flux–dependent river incision:  
751 Implications for extracting tectonic signals from river profiles. *Geology*,  
752 36(7), 535. <https://doi.org/10.1130/G24681A.1>

753 Cramer, F. (2018). Scientific colour maps, Zenodo,  
754 doi:10.5281/zenodo.1243862

755 DiBiase, R. A., Denn, A. R., Bierman, P. R., Kirby, E., West, N., & Hidy, A. J.  
756 (2018a). Stratigraphic control of landscape response to base-level fall,  
757 Young Womans Creek, Pennsylvania, USA. *Earth and Planetary Science*  
758 *Letters*, 504, 163–173. <https://doi.org/10.1016/j.epsl.2018.10.005>

759 DiBiase, R. A., Rossi, M. W., & Neely, A. B. (2018b). Fracture density and  
760 grain size controls on the relief structure of bedrock landscapes.  
761 *Geology*, 46(5), 399–402. <https://doi.org/10.1130/G40006.1>

762 Duvall, A., Kirby, E., & Burbank, D. (2004). Tectonic and lithologic controls  
763 on bedrock channel profiles and processes in coastal California. *Journal*  
764 *of Geophysical Research: Earth Surface*, 109(F3), 2003JF000086.  
765 <https://doi.org/10.1029/2003JF000086>

766 Fernandez-Luque, R. & van Beek, R. (1976) Erosion and transport of bed-  
767 load sediment. *Journal of Hydraulic Research*, 14, 127–144.  
768 <https://doi.org/10.1080/00221687609499677>

769 Finnegan, N. J., Klier, R. A., Johnstone, S., Pfeiffer, A. M., & Johnson, K.  
770 (2017). Field evidence for the control of grain size and sediment supply  
771 on steady-state bedrock river channel slopes in a tectonically active  
772 setting. *Earth Surface Processes and Landforms*, 42(14), 2338–2349.  
773 <https://doi.org/10.1002/esp.4187>

774 Forte, A. M., Yanites, B. J., & Whipple, K. X. (2016). Complexities of  
775 landscape evolution during incision through layered stratigraphy with  
776 contrasts in rock strength. *Earth Surface Processes and Landforms*,  
777 41(12), 1736–1757. <https://doi.org/10.1002/esp.3947>

778 Fujii, K. (1981) Geology of the Abukuma District. Quadrangle Series, Scale  
779 1:50,000, Geological Survey of Japan, 38p.

780 Geological Survey of Japan, AIST (2023) Seamless digital geological map of  
781 Japan V2 1:200,000, Original edition. <https://gbank.gsj.jp/seamless/>  
782 [Accessed: Jul. 20th, 2024]

783 Guryan, G. J., Johnson, J. P. L., & Gasparini, N. M. (2024). Sediment Cover  
784 Modulates Landscape Erosion Patterns and Channel Steepness in  
785 Layered Rocks: Insights From the SPACE Model. *Journal of Geophysical*  
786 *Research: Earth Surface*, 129(7),  
787 e2023JF007509.<https://doi.org/10.1029/2023JF007509>

788 Hack, J.T. (1957) Studies of Longitudinal Stream Profiles in Virginia and  
789 Maryland. *United States Geological Survey Professional paper*, 294-B,  
790 45–97. <https://doi.org/10.3133/pp294B>

791 Hack, J.T. (1973) Stream-profile analysis and stream-gradient index. *Journal*  
792 *of Research of the U. S. Geological Survey*, 1(4), 421–429.

793 Harel, M.-A., Mudd, S. M., & Attal, M. (2016). Global analysis of the stream  
794 power law parameters based on worldwide <sup>10</sup>Be denudation rates.  
795 *Geomorphology*, 268, 184–196.  
796 <https://doi.org/10.1016/j.geomorph.2016.05.035>

797 The headquarters for earthquake research promotion (2004) On the long-  
798 term evaluation of the western marginal fault zone of the Aomori bay.  
799 [https://www.jishin.go.jp/main/chousa/katsudansou\\_pdf/09\\_aomori-](https://www.jishin.go.jp/main/chousa/katsudansou_pdf/09_aomori-wan.pdf)  
800 [wan.pdf](https://www.jishin.go.jp/main/chousa/katsudansou_pdf/09_aomori-wan.pdf) [Accessed:Aug. 15th, 2024]

801 Hodge, R. A., Voepel, H., Leyland, J., Sear, D. A., & Ahmed, S. (2020). X-  
802 ray computed tomography reveals that grain protrusion controls critical  
803 shear stress for entrainment of fluvial gravels. *Geology*, 48(2), 149–  
804 153. <https://doi.org/10.1130/G46883.1>

805 Hodge, R. A., Voepel, H. E., Yager, E. M., Leyland, J., Johnson, J. P. L., Sear,  
806 D. A., & Ahmed, S. (2024). Improving predictions of critical shear stress  
807 in gravel bed rivers: Identifying the onset of sediment transport and  
808 quantifying sediment structure. *Earth Surface Processes and Landforms*,  
809 49(8), 2517–2537. <https://doi.org/10.1002/esp.5842>

810 Howard, A. D., & Kerby, G. (1983). Channel changes in badlands. *Geological*  
811 *Society of America Bulletin*, 94(6), 739. [https://doi.org/10.1130/0016-  
812 7606\(1983\)94<739:CCIB>2.0.CO;2](https://doi.org/10.1130/0016-7606(1983)94<739:CCIB>2.0.CO;2)

813 Hurst, M. D., Mudd, S. M., Walcott, R., Attal, M., & Yoo, K. (2012). Using  
814 hilltop curvature to derive the spatial distribution of erosion rates.  
815 *Journal of Geophysical Research: Earth Surface*, 117(F2),  
816 2011JF002057. <https://doi.org/10.1029/2011JF002057>

817 Inoue, T., Izumi, N., Shimizu, Y., & Parker, G. (2014). Interaction among  
818 alluvial cover, bed roughness, and incision rate in purely bedrock and  
819 alluvial-bedrock channel. *Journal of Geophysical Research: Earth*  
820 *Surface*, 119(10), 2123–2146. <https://doi.org/10.1002/2014JF003133>

821 Johnson, J. P. L., Whipple, K. X., Sklar, L. S., & Hanks, T. C. (2009).  
822 Transport slopes, sediment cover, and bedrock channel incision in the



823 Henry Mountains, Utah. *Journal of Geophysical Research: Earth Surface*,  
824 114(F2), 2007JF000862. <https://doi.org/10.1029/2007JF000862>

825 Johnson, J. P. L., & Whipple, K. X. (2010). Evaluating the controls of shear  
826 stress, sediment supply, alluvial cover, and channel morphology on  
827 experimental bedrock incision rate. *Journal of Geophysical Research:*  
828 *Earth Surface*, 115(F2), 2009JF001335.  
829 <https://doi.org/10.1029/2009JF001335>

830 Kirby, E., Whipple, K. X., Tang, W., & Chen, Z. (2003). Distribution of active  
831 rock uplift along the eastern margin of the Tibetan Plateau: Inferences  
832 from bedrock channel longitudinal profiles. *Journal of Geophysical*  
833 *Research: Solid Earth*, 108(B4), 2001JB000861.  
834 <https://doi.org/10.1029/2001JB000861>

835 Lai, L. S., Roering, J. J., Finnegan, N. J., Dorsey, R. J., & Yen, J. (2021).  
836 Coarse sediment supply sets the slope of bedrock channels in rapidly  
837 uplifting terrain: Field and topographic evidence from eastern Taiwan.  
838 *Earth Surface Processes and Landforms*, 46(13), 2671–2689.  
839 <https://doi.org/10.1002/esp.5200>

840 Lamb, M. P., Dietrich, W. E., & Venditti, J. G. (2008). Is the critical Shields  
841 stress for incipient sediment motion dependent on channel-bed slope?  
842 *Journal of Geophysical Research: Earth Surface*, 113(F2),  
843 2007JF000831. <https://doi.org/10.1029/2007JF000831>

844 Leonard, J. S., Whipple, K. X., & Heimsath, A. M. (2023). Isolating climatic,  
845 tectonic, and lithologic controls on mountain landscape evolution.  
846 *Science Advances*, 9(3), eadd8915.  
847 <https://doi.org/10.1126/sciadv.add8915>

848 Liébault, F., Piégay, H., Cassel, M., & Arnaud, F. (2024). Bedload tracing  
849 with RFID tags in gravel-bed rivers: Review and meta-analysis after 20  
850 years of field and laboratory experiments. *Earth Surface Processes and*  
851 *Landforms*, 49(1), 147–169. <https://doi.org/10.1002/esp.5704>

852 MacKenzie, L. G., & Eaton, B. C. (2017). Large grains matter: Contrasting  
853 bed stability and morphodynamics during two nearly identical  
854 experiments. *Earth Surface Processes and Landforms*, 42(8), 1287–  
855 1295. <https://doi.org/10.1002/esp.4122>

856 MacKenzie, L. G., Eaton, B. C., & Church, M. (2018). Breaking from the  
857 average: Why large grains matter in gravel-bed streams. *Earth Surface*  
858 *Processes and Landforms*, 43(15), 3190–3196.  
859 <https://doi.org/10.1002/esp.4465>

860 Mimura, T. (1979) On the development of the geological structure in the  
861 southern part of the Tsugaru peninsula, Aomori Prefecture. *Journal of*  
862 *Geological Society of Japan*, 85(12), 719–735.  
863 <https://doi.org/10.5575/geosoc.85.719>

864 Mishra, J., & Inoue, T. (2020). Alluvial cover on bedrock channels:  
865       Applicability of existing models. *Earth Surface Dynamics*, 8(3), 695–  
866       716. <https://doi.org/10.5194/esurf-8-695-2020>

867 Molnar, P., Anderson, R. S., & Anderson, S. P. (2007). Tectonics, fracturing  
868       of rock, and erosion. *Journal of Geophysical Research: Earth Surface*,  
869       112(F3), 2005JF000433. <https://doi.org/10.1029/2005JF000433>

870 Montgomery, D. R., & Gran, K. B. (2001). Downstream variations in the  
871       width of bedrock channels. *Water Resources Research*, 37(6), 1841–  
872       1846. <https://doi.org/10.1029/2000WR900393>

873 Montgomery, D. R., & Brandon, M. T. (2002). Topographic controls on  
874       erosion rates in tectonically active mountain ranges. *Earth and*  
875       *Planetary Science Letters*, 201(3–4), 481–489.  
876       [https://doi.org/10.1016/S0012-821X\(02\)00725-2](https://doi.org/10.1016/S0012-821X(02)00725-2)

877 Nakata, T. & Imaizumi, T. (Eds.) (2002) Digital active fault map of Japan.  
878       University of Tokyo press.

879 Nemoto, N. (2014) Neogene to Quaternary tectonics in the Tsugaru  
880       Peninsula, northeast Japan. *The Quaternary Research*, 53(4), 205–212.  
881       <https://doi.org/10.4116/jaqua.53.205>

882 Perne, M., Covington, M. D., Thaler, E. A., & Myre, J. M. (2017). Steady  
883       state, erosional continuity, and the topography of landscapes developed  
884       in layered rocks. *Earth Surface Dynamics*, 5(1), 85–100.  
885       <https://doi.org/10.5194/esurf-5-85-2017>

886 Perret, E., Camenen, B., Berni, C., El Kadi Abderrezzak, K., & Renard, B.  
887 (2023). Uncertainties in Models Predicting Critical Bed Shear Stress of  
888 Cohesionless Particles. *Journal of Hydraulic Engineering*, 149(4),  
889 04023002. <https://doi.org/10.1061/JHEND8.HYENG-13101>

890 Petit, F., Houbrechts, G., Peeters, A., Hallot, E., Van Campenhout, J., &  
891 Denis, A.-C. (2015). Dimensionless critical shear stress in gravel-bed  
892 rivers. *Geomorphology*, 250, 308–320.  
893 <https://doi.org/10.1016/j.geomorph.2015.09.008>

894 Phillips, C. B., Masteller, C. C., Slater, L. J., Dunne, K. B. J., Francalanci, S.,  
895 Lanzoni, S., Merritts, D. J., Lajeunesse, E., & Jerolmack, D. J. (2022).  
896 Threshold constraints on the size, shape and stability of alluvial rivers.  
897 *Nature Reviews Earth & Environment*, 3(6), 406–419.  
898 <https://doi.org/10.1038/s43017-022-00282-z>

899 Rice, S. (1998). Which tributaries disrupt downstream fining along gravel-  
900 bed rivers? *Geomorphology*, 22(1), 39–56.  
901 [https://doi.org/10.1016/S0169-555X\(97\)00052-4](https://doi.org/10.1016/S0169-555X(97)00052-4)

902 Rice, S., & Church, M. (1998). Grain size along two gravel-bed rivers:  
903 Statistical variation, spatial pattern and sedimentary links. *Earth*  
904 *Surface Processes and Landforms*, 23(4), 345–363.  
905 [https://doi.org/10.1002/\(SICI\)1096-9837\(199804\)23:4<345::AID-  
906 ESP850>3.0.CO;2-B](https://doi.org/10.1002/(SICI)1096-9837(199804)23:4<345::AID-ESP850>3.0.CO;2-B)

907 Roda-Boluda, D. C., D'Arcy, M., McDonald, J., & Whittaker, A. C. (2018).  
908 Lithological controls on hillslope sediment supply: Insights from  
909 landslide activity and grain size distributions. *Earth Surface Processes  
910 and Landforms*, 43(5), 956–977. <https://doi.org/10.1002/esp.4281>

911 Roering, J. J., Kirchner, J. W., & Dietrich, W. E. (2001). Hillslope evolution  
912 by nonlinear, slope-dependent transport: Steady state morphology and  
913 equilibrium adjustment timescales. *Journal of Geophysical Research:  
914 Solid Earth*, 106(B8), 16499–16513.  
915 <https://doi.org/10.1029/2001JB000323>

916 Scheingross, J. S., Brun, F., Lo, D. Y., Omerdin, K., & Lamb, M. P. (2014).  
917 Experimental evidence for fluvial bedrock incision by suspended and  
918 bedload sediment. *Geology*, 42(6), 523–526.  
919 <https://doi.org/10.1130/G35432.1>

920 Schwanghart, W., & Scherler, D. (2014). Short Communication:  
921 TopoToolbox 2 – MATLAB-based software for topographic analysis and  
922 modeling in Earth surface sciences. *Earth Surface Dynamics*, 2(1), 1–7.  
923 <https://doi.org/10.5194/esurf-2-1-2014>

924 Shobe, C. M., Tucker, G. E., & Barnhart, K. R. (2017). The SPACE 1.0  
925 model: A Landlab component for 2-D calculation of sediment transport,  
926 bedrock erosion, and landscape evolution. *Geoscientific Model  
927 Development*, 10(12), 4577–4604. [https://doi.org/10.5194/gmd-10-  
928 4577-2017](https://doi.org/10.5194/gmd-10-4577-2017)

929 Shobe, C. M., Bennett, G. L., Tucker, G. E., Roback, K., Miller, S. R., &  
930 Roering, J. J. (2021a). Boulders as a lithologic control on river and  
931 landscape response to tectonic forcing at the Mendocino triple junction.  
932 *GSA Bulletin*, 133(3–4), 647–662. <https://doi.org/10.1130/B35385.1>

933 Shobe, C. M., Turowski, J. M., Nativ, R., Glade, R. C., Bennett, G. L., & Dini,  
934 B. (2021b). The role of infrequently mobile boulders in modulating  
935 landscape evolution and geomorphic hazards. *Earth-Science Reviews*,  
936 220, 103717. <https://doi.org/10.1016/j.earscirev.2021.103717>

937 Sklar, L. S., & Dietrich, W. E. (2001). Sediment and rock strength controls  
938 on river incision into bedrock. *Geology*, 29(12), 1087.  
939 [https://doi.org/10.1130/0091-](https://doi.org/10.1130/0091-7613(2001)029<1087:SARSCO>2.0.CO;2)  
940 [7613\(2001\)029<1087:SARSCO>2.0.CO;2](https://doi.org/10.1130/0091-7613(2001)029<1087:SARSCO>2.0.CO;2)

941 Sklar, L. S., & Dietrich, W. E. (2004). A mechanistic model for river incision  
942 into bedrock by saltating bed load. *Water Resources Research*, 40(6),  
943 2003WR002496. <https://doi.org/10.1029/2003WR002496>

944 Sklar, L. S., & Dietrich, W. E. (2006). The role of sediment in controlling  
945 steady-state bedrock channel slope: Implications of the saltation–  
946 abrasion incision model. *Geomorphology*, 82(1–2), 58–83.  
947 <https://doi.org/10.1016/j.geomorph.2005.08.019>

948 Sklar, L. S., Riebe, C. S., Marshall, J. A., Genetti, J., Leclere, S., Lukens, C.  
949 L., & Merces, V. (2017). The problem of predicting the size distribution

950 of sediment supplied by hillslopes to rivers. *Geomorphology*, 277, 31–  
951 49. <https://doi.org/10.1016/j.geomorph.2016.05.005>

952 Sklar, L. S. (2024). Grain Size in Landscapes. *Annual Review of Earth and*  
953 *Planetary Sciences*, 52(1), 663–692. [https://doi.org/10.1146/annurev-](https://doi.org/10.1146/annurev-earth-052623-075856)  
954 [earth-052623-075856](https://doi.org/10.1146/annurev-earth-052623-075856)

955 Smith, H. E. J., Monsalve, A. D., Turowski, J. M., Rickenmann, D., & Yager,  
956 E. M. (2023). Controls of local grain size distribution, bed structure and  
957 flow conditions on sediment mobility. *Earth Surface Processes and*  
958 *Landforms*, 48(10), 1990–2004. <https://doi.org/10.1002/esp.5599>

959 Snyder, N. P. (2000). Landscape response to tectonic forcing: Digital  
960 elevation model analysis of stream profiles in the Mendocino triple  
961 junction region, northern California. *Geological Society of America*  
962 *Bulletin*.

963 Stock, J., & Dietrich, W. E. (2003). Valley incision by debris flows: Evidence  
964 of a topographic signature. *Water Resources Research*, 39(4),  
965 2001WR001057. <https://doi.org/10.1029/2001WR001057>

966 Suzuki, T., Eden, D., Danhara, T., & Fujiwara, O. (2005). Correlation of the  
967 Hakkoda–Kokumoto Tephra, a widespread Middle Pleistocene tephra  
968 erupted from the Hakkoda Caldera, northeast Japan. *Island Arc*, 14(4),  
969 666–678. <https://doi.org/10.1111/j.1440-1738.2005.00475.x>

970 Takahashi, N., Shyu, J. B. H., Chen, C.-Y., & Toda, S. (2022). Long-term  
971 uplift pattern recorded by rivers across contrasting lithology: Insights

972 into earthquake recurrence in the epicentral area of the 2016  
973 Kumamoto earthquake, Japan. *Geomorphology*, 419, 108492.  
974 <https://doi.org/10.1016/j.geomorph.2022.108492>

975 Takahashi, N. O., Shyu, J. B. H., Toda, S., Matsushi, Y., Ohta, R. J., &  
976 Matsuzaki, H. (2023). Transient Response and Adjustment Timescales  
977 of Channel Width and Angle of Valley-Side Slopes to Accelerated  
978 Incision. *Journal of Geophysical Research: Earth Surface*, 128(8),  
979 e2022JF006967. <https://doi.org/10.1029/2022JF006967>

980 Thaler, E. A., & Covington, M. D. (2016). The influence of sandstone caprock  
981 material on bedrock channel steepness within a tectonically passive  
982 setting: Buffalo National River Basin, Arkansas, USA. *Journal of*  
983 *Geophysical Research: Earth Surface*, 121(9), 1635–1650.  
984 <https://doi.org/10.1002/2015JF003771>

985 Tsushima, K. & Uemura, F. (1959) Explanatory text of the geological map of  
986 Japan, Scale 1:50000, Kodomari. Geological Survey of Japan, 43p.

987 Turowski, J. M., Lague, D., & Hovius, N. (2007). Cover effect in bedrock  
988 abrasion: A new derivation and its implications for the modeling of  
989 bedrock channel morphology. *Journal of Geophysical Research: Earth*  
990 *Surface*, 112(F4), 2006JF000697.  
991 <https://doi.org/10.1029/2006JF000697>

992 Turowski, J. M., Pruß, G., Voigtländer, A., Ludwig, A., Landgraf, A., Kober,  
993 F., & Bonnelye, A. (2023). Geotechnical controls on erodibility in fluvial



994 impact erosion. *Earth Surface Dynamics*, 11(5), 979–994.  
995 <https://doi.org/10.5194/esurf-11-979-2023>

996 Uemura, F. (1959) Explanatory text of the geological map of Japan, Scale  
997 1:50000, Kodomari. Geological Survey of Japan, 39p.

998 Ujiie, Y., Taniguchi, T., Ebina, M. (2006) Evaluation of the displacement of  
999 the Tsugaru Fault by means of organic maturity of fossil pollen in  
1000 sediments. *Journal of Geological Society of Japan*, 112(10), 581–593.  
1001 <https://doi.org/10.5575/geosoc.112.581>

1002 Vázquez-Tarrío, D., Recking, A., Liébault, F., Tal, M., & Menéndez-Duarte, R.  
1003 (2019). Particle transport in gravel-bed rivers: Revisiting passive tracer  
1004 data. *Earth Surface Processes and Landforms*, 44(1), 112–128.  
1005 <https://doi.org/10.1002/esp.4484>

1006 Verdian, J. P., Sklar, L. S., Riebe, C. S., & Moore, J. R. (2021). Sediment  
1007 size on talus slopes correlates with fracture spacing on bedrock cliffs:  
1008 Implications for predicting initial sediment size distributions on  
1009 hillslopes. *Earth Surface Dynamics*, 9(4), 1073–1090.  
1010 <https://doi.org/10.5194/esurf-9-1073-2021>

1011 Whipple, K. X., & Tucker, G. E. (1999). Dynamics of the stream-power river  
1012 incision model: Implications for height limits of mountain ranges,  
1013 landscape response timescales, and research needs. *Journal of*  
1014 *Geophysical Research: Solid Earth*, 104(B8), 17661–17674.  
1015 <https://doi.org/10.1029/1999JB900120>

1016 Whipple, K. X., & Tucker, G. E. (2002). Implications of sediment-flux-  
1017 dependent river incision models for landscape evolution. *Journal of*  
1018 *Geophysical Research: Solid Earth*, 107(B2).  
1019 <https://doi.org/10.1029/2000JB000044>

1020 Whittaker, A. C., Cowie, P. A., Attal, M., Tucker, G. E., & Roberts, G. P.  
1021 (2007). Contrasting transient and steady-state rivers crossing active  
1022 normal faults: New field observations from the Central Apennines, Italy.  
1023 *Basin Research*, 19(4), 529–556. [https://doi.org/10.1111/j.1365-](https://doi.org/10.1111/j.1365-2117.2007.00337.x)  
1024 [2117.2007.00337.x](https://doi.org/10.1111/j.1365-2117.2007.00337.x)

1025 Yanites, B. J. (2018). The Dynamics of Channel Slope, Width, and Sediment  
1026 in Actively Eroding Bedrock River Systems. *Journal of Geophysical*  
1027 *Research: Earth Surface*, 123(7), 1504–1527.  
1028 <https://doi.org/10.1029/2017JF004405>

1029 Yanites, B. J., Becker, J. K., Madritsch, H., Schnellmann, M., & Ehlers, T. A.  
1030 (2017). Lithologic Effects on Landscape Response to Base Level  
1031 Changes: A Modeling Study in the Context of the Eastern Jura  
1032 Mountains, Switzerland. *Journal of Geophysical Research: Earth*  
1033 *Surface*, 122(11), 2196–2222. <https://doi.org/10.1002/2016JF004101>  
1034